ACS APPLIED MATERIALS & INTERFACES

Research Article

www.acsami.org

Tunable Morphology Synthesis of $LiFePO_4$ Nanoparticles as Cathode Materials for Lithium Ion Batteries

Zhipeng Ma,[†,‡] Guangjie Shao,*[,†,‡] Yuqian Fan,[†,‡] Guiling Wang,[†,‡] Jianjun Song,[†,‡] and Tingting Liu[†,‡]

[†]State Key Laboratory of Metastable Materials Science and Technology, Yanshan University, Qinhuangdao 066004, China

[‡]Hebei Key Laboratory of Applied Chemistry, College of Environmental and Chemical Engineering, Yanshan University, Qinhuangdao 066004, China

Supporting Information

ABSTRACT: Olivine $LiFePO_4$ with nanoplate, rectangular prism nanorod and hexagonal prism nanorod morphologies with a short *b*-axis were successfully synthesized by a solvothermal in glycerol and water system. The influences of solvent composition on the morphological transformation and electrochemical performances of olivine $LiFePO_4$ are systematically investigated by X-ray diffraction, scanning electron microscopy, transmission electron microscopy and galvanostatic charge−discharge tests. It is found that with increasing water content in solvent, the $LiFePO_4$ nanoplates gradually transform into hexagonal prism nanorods that are similar to the thermodynamic equilibrium shape of the $LiFePO_4$ crystal. This indicates that water plays an important role in the morphology transformation of the olivine $LiFePO_4$. The electrochemical performances vary significantly with the particle morphology. The $LiFePO_4$ rectangular prism nanorods (formed in a glycerol-to-water ratio of 1:1) exhibit superior electrochemical properties compared with the other morphological particles because of their moderate size and shorter Li^+ ion diffusion length along the [010] direction. The initial discharge capacity of the $LiFePO_4$@C with a rectangular prism nanorod morphology reaches to 163.8 mAh g^{-1} at 0.2 C and over 75 mAh g^{-1} at the high discharging rate of 20 C, maintaining good stability at each discharging rate.

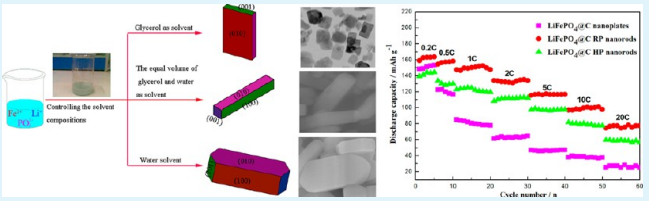

KEYWORDS: *lithium iron phosphates, shape controlled nanoparticles, solvothermal, electrochemical performance, lithium ion batteries*

1. INTRODUCTION

The high power Li ion rechargeable battery has attracted vast attention all over the world for its application in hybrid electric vehicles (HEVs) and electric vehicles (EVs). Olivine structured $LiFePO_4$ is one of the most promising cathode materials for next-generation Li ion batteries in large-size and high-rate applications.[1] It possesses excellent chemical and thermal stability, an acceptable flat voltage plateau (3.4 V vs Li^+/Li), and a high theoretical rate capacity of 170 mAh g^{-1}, and it offers economic and environmental advantages because it is a kind of low-cost and nontoxic material.[2−8] Although $LiFePO_4$ has been applied to practical uses, there is still a long way to go. For example, the high-rate and low-temperature performances of the cells are not satisfied. The main obstacles for applicable electrochemical performances are its poor electronic conductivity and lithium ion diffusivity.[9] Enormous attempts have been made to overcome the drawbacks, for instance, coating with conductive carbon or conductive polymers,[10−17] doping with aliovalent cation,[18,19] controlling particle morphologies[20] and preparing nanosized particles.[21]

It is widely recognized that the electrochemical performances of $LiFePO_4$ particles are closely related to their morphologies and crystal orientations.[22,23] Hydrothermal synthesis techniques have been used to prepare olivine $LiFePO_4$ with a variety of particle morphologies and sizes at low temperature. For instance, $LiFePO_4$ nano-microspheres self-assembled by the ordered nanoplates have been synthesized by a hydrothermal method using phytic acid as the phosphorus source.[24] Similarly, $LiFePO_4$ microspheres with an enhanced tap density were assembled from nanoplates via solvothermal treatment with TiN nanoparticles as a conductive connector.[25] $LiFePO_4$ crystallites have also been synthesized with platet,[26,27] nanorod,[28−30] mesoporous microsphere,[31,32] flower-like,[33,34] dumbbell-like,[35] hollow-like,[36,37] nest-like,[38] and cage-like[39] structures. The anisotropic morphologies of the particles are highly dependent on the experimental conditions, for example, the addition of component in the solvent such as propanediol, ethylene glycol (EG),[23,38] polyvinylpyrrolidone (PVP),[30] and poly(ethylene glycol) 400 (PEG400),[27] etc. which in particular act as shape controllers. Besides, computational[40,41] and experimental[42] studies of $LiFePO_4$ have indicated that charge transfer mainly takes place on the *ac*-facet, and Li^+ ion migration occurs preferentially via one dimensional channels oriented along the [010] direction of the orthorhombic crystal structure during charge and discharge. Thus, nanorods and nanoplates with a short *b*-axis are ideal structures for good electrochemical performance of $LiFePO_4$. Although considerable progress has been made in the synthesis of $LiFePO_4$,

Received: March 7, 2014
Accepted: May 22, 2014
Published: May 22, 2014

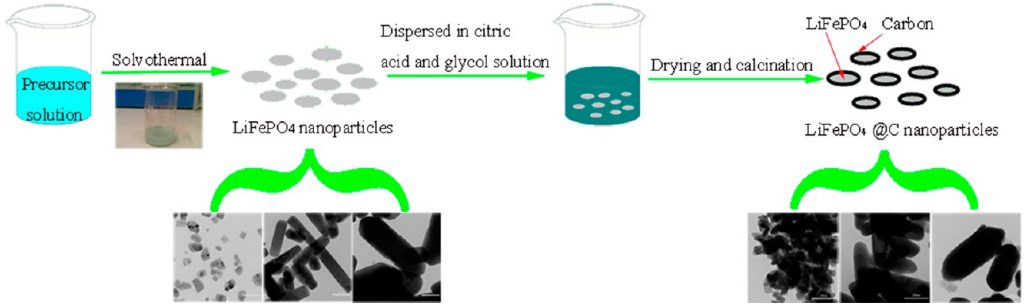

Figure 1. Schematic illustration of the preparation process for the $LiFePO_4$@C core−shell nanoparticles.

numerous questions related to the fundamental forming mechanism of $LiFePO_4$ with various morphologies remain unanswered.

In this paper, we report a simple solvothermal method to fabricate $LiFePO_4$ nanoplates with a large (010) plane and $LiFePO_4$ rectangular prism and hexagonal prism nanorods with a short *b*-axis by controlling solvent composition. The effects of solvent composition on the morphological transformation and electrochemical performances of olivine $LiFePO_4$ have been discussed in detail. Furthermore, the formation mechanism of $LiFePO_4$ with various morphologies is proposed.

2. EXPERIMENTAL SECTION

2.1. Material Preparation and Characterization. $LiFePO_4$ rectangular prism nanorods were prepared by a solvothermal route, with glycerol and water as the reaction medium solvent. For a typical synthesis, 0.045 mol $LiOH·H_2O$ was dissolved in 20 mL of glycerol and water (the volume ratio of glycerol and water is 1:1).

Then 0.015 mol H_3PO_4 was added to the LiOH solution under stirring to form a white deposition. Next, 0.015 mol $FeSO_4·7H_2O$ dissolved in 20 mL of glycerol and water (the volume ratio of glycerol and water is 1:1) was dropped into the above suspension with vigorous magnetic stirring for 30 min. The precursor was transferred into a Teflon-lined autoclave (inner volume: 100 mL) and heated to 180 °C for 18 h and then cooled down to room temperature. The obtained precipitate was filtered and washed several times with distilled water and ethanol, and dried at 80 °C for 12 h.

For the synthesis of $LiFePO_4$ nanoplates and hexagonal prism nanorods, the procedures were kept unchanged except that the volume ratios of glycerol and water are 2:0 and 0:2, respectively.

To improve the electrochemical performances, the $LiFePO_4$ nanopowders were coated with carbon film on the surface to form $LiFePO_4$@C core−shell nanostructures. The coating procedures are as follows: $LiFePO_4$ nanopowders and a proper amount of ethylene glycol were added to 10 mL of citric acid solution under stirring, and then the solution was evaporated to obtain a dark blue gel at 80 °C in water bath. After that, the gel was carbonized for 6 h at 700 °C in nitrogen atmosphere to obtain the carbon film. The schematic illustration of the typical experiment process is shown in Figure 1.

The structure of the as-prepared samples was characterized by X-ray diffraction (XRD) on a Rigaku D/max-2500/pc. The morphology and microstructure of the powders were observed by field-emission scanning electron microscopy (FE-SEM) on an S-4800 FE-SEM and high-resolution transmission electron microscopy (HRTEM) with model JEM2010.

2.2. Cell Fabrication and Electrochemical Analysis. The electrochemical performances of the samples were measured in a simulative cell, which consisted of a working electrode and a lithium foil electrode separated by a Celgard 2400 microporous membrane. The working electrode was prepared by dispersing 80 wt % active materials, 10 wt % acetylene black, and 10 wt % polyvinylidene fluoride (PVDF) binder in the *N*-methylpyrrolidione (NMP) solvent to form a uniform slurry. The slurry was coated on Al foils and dried in a vacuum at 120 °C for 12 h. The electrolyte was 1 M $LiPF_6$/EC+DEC (1:1, v/v). The cells were assembled in an argon-filled glovebox and tested by galvanostatic charge−discharge cycling in the voltage ranges of 2.4−4.2 V on a battery testing system (LAND, Wuhan, China). The electrochemical impedance spectra (EIS) test (the frequency range of 0.01−100 000 Hz) was performed on a ParStat 4000 electrochemical workstation.

3. RESULTS AND DISCUSSION

3.1. Morphology of the Prepared $LiFePO_4$. Figure 2 shows the XRD patterns of the samples prepared in solvents

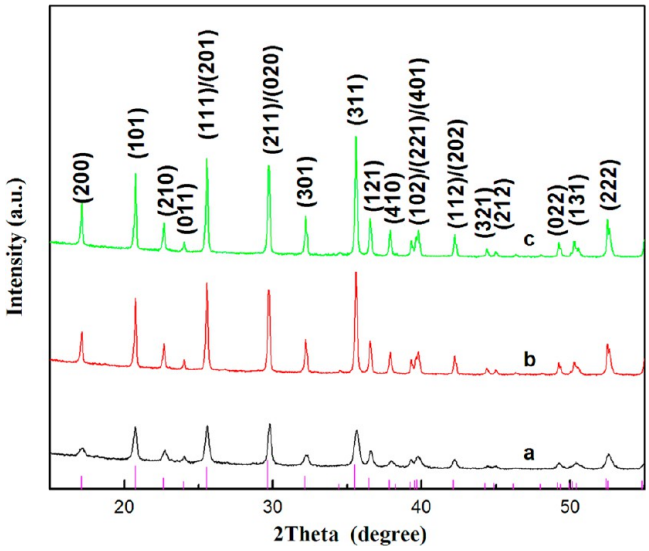

Figure 2. XRD patterns of these samples prepared in different solvent compositions with various volume ratios of glycerol to water of 2:0 (a), 1:1 (b), and 0:2 (c).

with various volume ratios of glycerol to water of 2:0, 1:1, and 0:2. It is very clear that all peaks of the $LiFePO_4$ samples obtained in different solvents can be well indexed to an orthorhombic olivine-type phase $LiFePO_4$ (JCPDS card No. 83-2092), indicating that the solvent composition has no effect on phase purity.

The SEM and TEM images of the $LiFePO_4$ samples prepared in solvents with different compositions are shown in Figure S1 (see the Supporting Information) and Figure 3a−c, respectively. It can be seen from Figure 3a that the material synthesized in the glycerol solvent is composed of nanoplates (<100 nm). The indexing of the selected area electron diffraction (SAED) pattern shown in Figure 3d suggests that each nanoplate is a $LiFePO_4$ single crystal with a large (010) plane. When the reaction solvent is composed of glycerol and water in the ratio of 1:1, the morphology of the material is

dx.doi.org/10.1021/am501373h | ACS Appl. Mater. Interfaces 2014, 6, 9236−9244

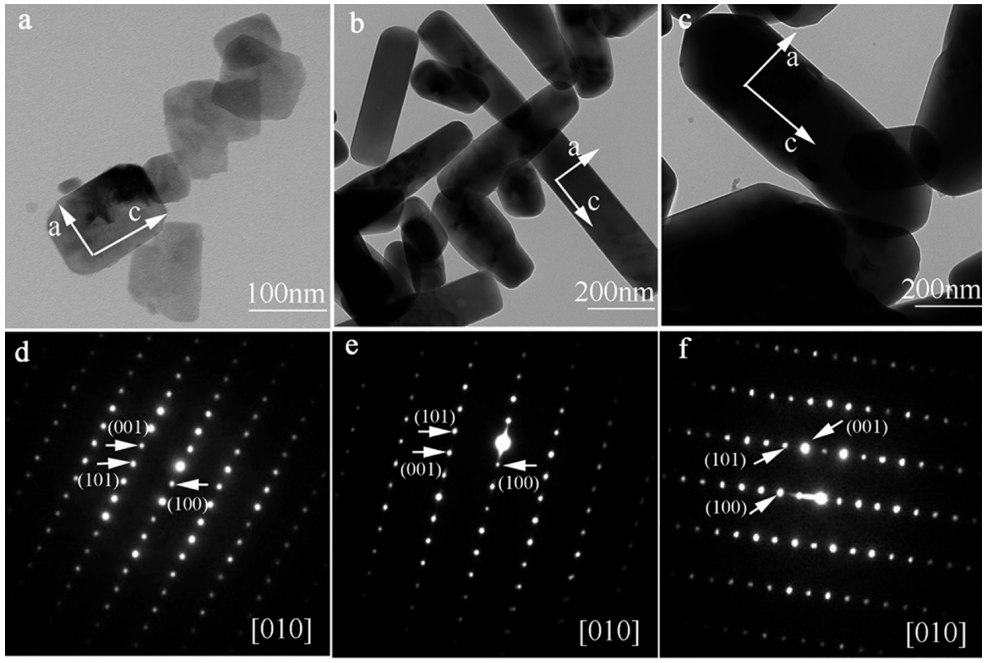

Figure 3. TEM and the corresponding SAED images of the $LiFePO_4$ nanoplates (a, d), rectangular prism-like nanorods (b, e) and hexagonal prism-like nanorods (c, f).

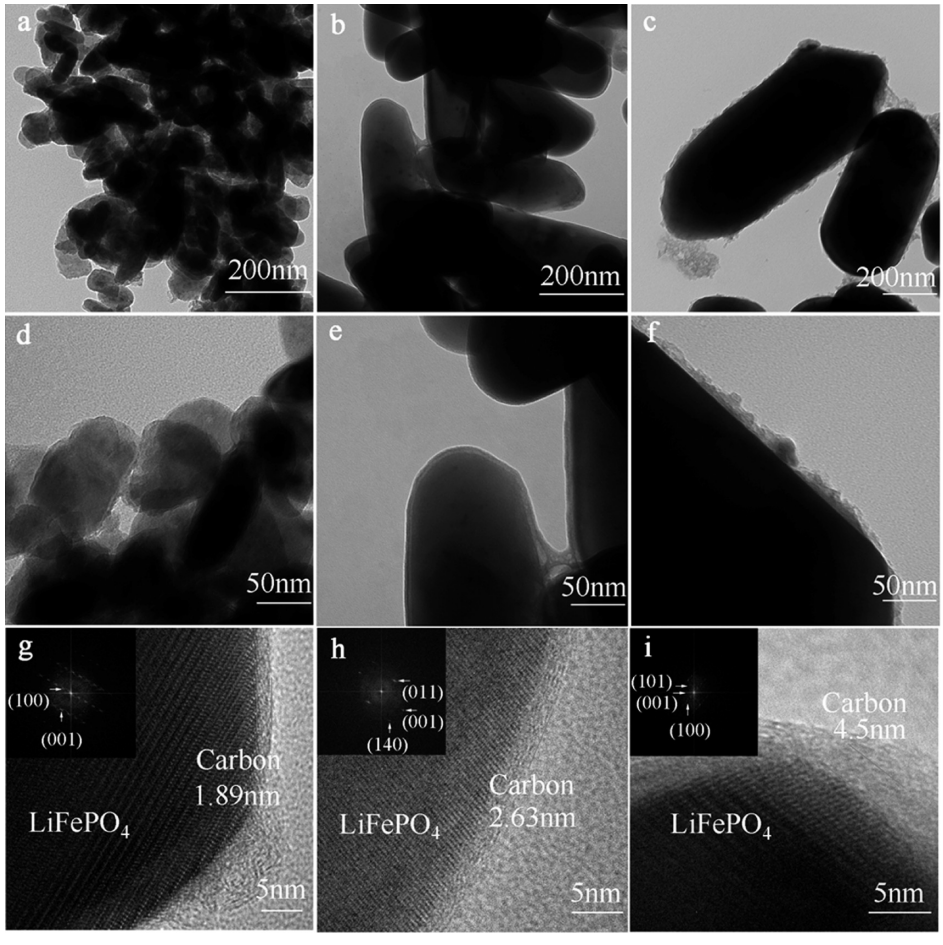

Figure 4. TEM and the corresponding HRTEM images of the $LiFePO_4$@C nanoplates (a, d, and g), rectangular prism-like nanorods (b, e, and h), and hexagonal prism-like nanorods (c, f, and (i). The inset images in g, h, and i are the corresponding fast Fourier transform pattern.

dx.doi.org/10.1021/am501373h | *ACS Appl. Mater. Interfaces* 2014, 6, 9236−9244

entirely transformed into rectangular prism nanorods with a short *b*-axis, as shown in Figure 3b,e. The mean diameter of the nanorods is 100 nm and the length is 500 nm. However, when the pure water is used as the solvent, as shown in Figure 3c, the $LiFePO_4$ is entirely changed to thicker hexagonal prism nanorods with a short *b*-axis. The morphologies of the $LiFePO_4$ after calcination and carbon-coating are shown in Figure 4a–c. It can be seen that the $LiFePO_4$@C composites still retain their original morphologies. Moreover, we can clearly see from Figure 4d–f that the wrap layers characterized by Raman spectra (Figure S2, see the Supporting Information for details) fully coated on the surface of $LiFePO_4$ nanoparticles. To better understand the coating carbon layer of $LiFePO_4$@C samples, the HRTEM images are presented in Figure 4g–i, showing that the thickness of the carbon coating layers for $LiFePO_4$@C nanoplates, rectangular prism nanorods, and hexagonal prism nanorods are ca. 1.89, 2.63, and 4.5 nm, respectively. In addition, the amount of the coated carbon on the $LiFePO_4$ samples is checked by TGA analysis, as shown in Figure S3 (see the Supporting Information for more details). The percentage of the coated carbon in $LiFePO_4$@C nanoplates, $LiFePO_4$@C rectangular prism-like nanorods and $LiFePO_4$@C hexagonal prism-like nanorods are ca. 3.4, 3.31, and 3.02 wt %, respectively. The above results indicate that the carbon coating layer becomes thicker with the increase of the $LiFePO_4$ grain size and the transformation of the morphology from nanoplates to hexagonal prism nanorods. The well-coated carbon layer on the surface of $LiFePO_4$ is favorable for the electrochemical performances of the materials.

Figure 5 shows the XRD patterns of the $LiFePO_4$@C nanoplates, rectangular prism nanorods and hexagonal prism

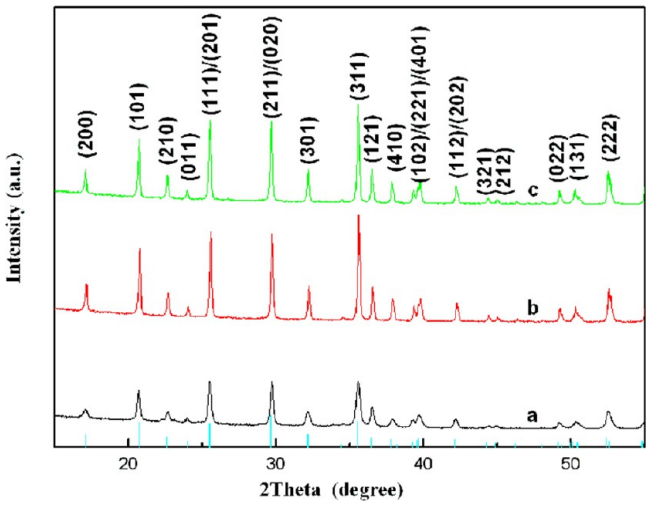

Figure 5. XRD patterns of $LiFePO_4$@C nanoplates (a), rectangular prism-like nanorods (b), and hexagonal prism-like nanorods (c).

nanorods. It is revealed that all the diffraction intensities of the prepared $LiFePO_4$@C composites become stronger after high temperature heat treatment, and no characteristic peaks of impurity phases are observed. In addition, the strong diffraction peaks and narrow half maximum (fwhm) of the XRD patterns indicate the highly crystallinity of $LiFePO_4$@C samples.

3.2. Electrochemical Properties of the Prepared $LiFePO_4$. Figure 6a–c shows the charge/discharge curves of the $LiFePO_4$@C samples within the first five cycles at a low current rate of 0.2 C. Obviously, the discharge capacity of the $LiFePO_4$@C rectangular prism nanorods (163.8 mAh g^{-1}) is much higher than those of the $LiFePO_4$@C nanoplates (153.3 mAh g^{-1}) and hexagonal prism nanorods (144.4 mAh g^{-1}). Moreover, from Figure 6a–c, it can be seen that the voltage differences between the charge and discharge flat plateau are 131, 110, and 142 mV for the $LiFePO_4$@C nanoplates, rectangular prism nanorods, and hexagonal prism nanorods, respectively. The $LiFePO_4$@C rectangular prism nanorods show the smallest voltage difference, indicating that it has the least polarization at a low current density.[43] The small polarization is related to the well-coated carbon layer on the surface of the $LiFePO_4$.[43−45] Figure 6d shows the comparison of the rate performance of the $LiFePO_4$@C nanoplates, rectangular prism nanorods, and hexagonal prism nanorods. The $LiFePO_4$@C rectangular prism nanorods exhibit the highest discharge capacity within the discharge rate, ranging from 0.2 to 20 C, and maintain good stability at each rate. Its discharge capacities reach 163.8, 158.2, 150.2, 135.3, 117, 101.1, and 78.5 mAh g^{-1} at 0.2, 0.5, 1, 2, 5, 10, and 20 C, respectively. The capacity of the $LiFePO_4$@C nanoplates with the large (010) plane shows a similar degradation behavior but slightly lower discharge capacity than that of the $LiFePO_4$@C rectangular prism nanorods. The lower discharge capacity is due to the fact that the particle size of the $LiFePO_4$@C nanoplates is so small (<100 nm) that they contain a few Fe-antisite defects, which block the transportation of Li along the *b*-axis.[46] This factor declines the electrochemical performance of the $LiFePO_4$@C nanoplates with the (010) plane (<100 nm). For the $LiFePO_4$@C hexagonal prism nanorods, its poor discharge capacity and severe discharge degradation are resulted from the large size of the particles.

To further explain the electrochemical behaviors of the $LiFePO_4$@C nanoplate and the rectangular prism nanorod and hexagonal prism nanorod electrodes, the electrochemical kinetic performance of the three cathodes was analyzed with electrochemical impedance spectra (EIS) measurements. Figure 7 shows the Nyquist plots of the three electrodes measured after 2 cycles at the 50% of discharge state. Each spectrum consists of a depressed semicircle in a high frequency region and a slope in a low frequency region. The semicircle in the high frequency region is referred to be a measure of the charge-transfer resistance at the electrolyte/electrode interface.[47,48] The slope line in the low frequency region is attributed to the diffusion of the lithium ion in the bulk of the electrode material. As seen in Figure 7, the very small high frequency semicircle for the $LiFePO_4$@C rectangular prism nanorod electrode implies its low charge-transfer resistance (139.3 Ω) at the electrolyte/electrode interface. As for the $LiFePO_4$@C nanoplate and hexagonal prism nanorod electrodes, the charge-transfer resistance is calculated to be 240 and 658.5 Ω, respectively. These results are in good agreement with the difference in the rate performance of the three electrodes exhibited in Figure 6d.

3.3. Exploration in the Formation Mechanism of $LiFePO_4$ with Various Morphologies. To further investigate the effects of the solvent compositions on the morphology of $LiFePO_4$, the SEM and TEM images of the $LiFePO_4$ samples synthesized in solvent with different compositions are shown in Figure 8. It can be seen that when the ratio of glycerol to water is 2:0, $LiFePO_4$ nanopowders are composed of nanoplates (<100 nm), as shown in Figure 8a,b. These nanoplates have a large (010) plane judged from the HRTEM (high-resolution transmission electron microscope) image (inset image in Figure 8b). Once a thimbleful of water is introduced into the solvent

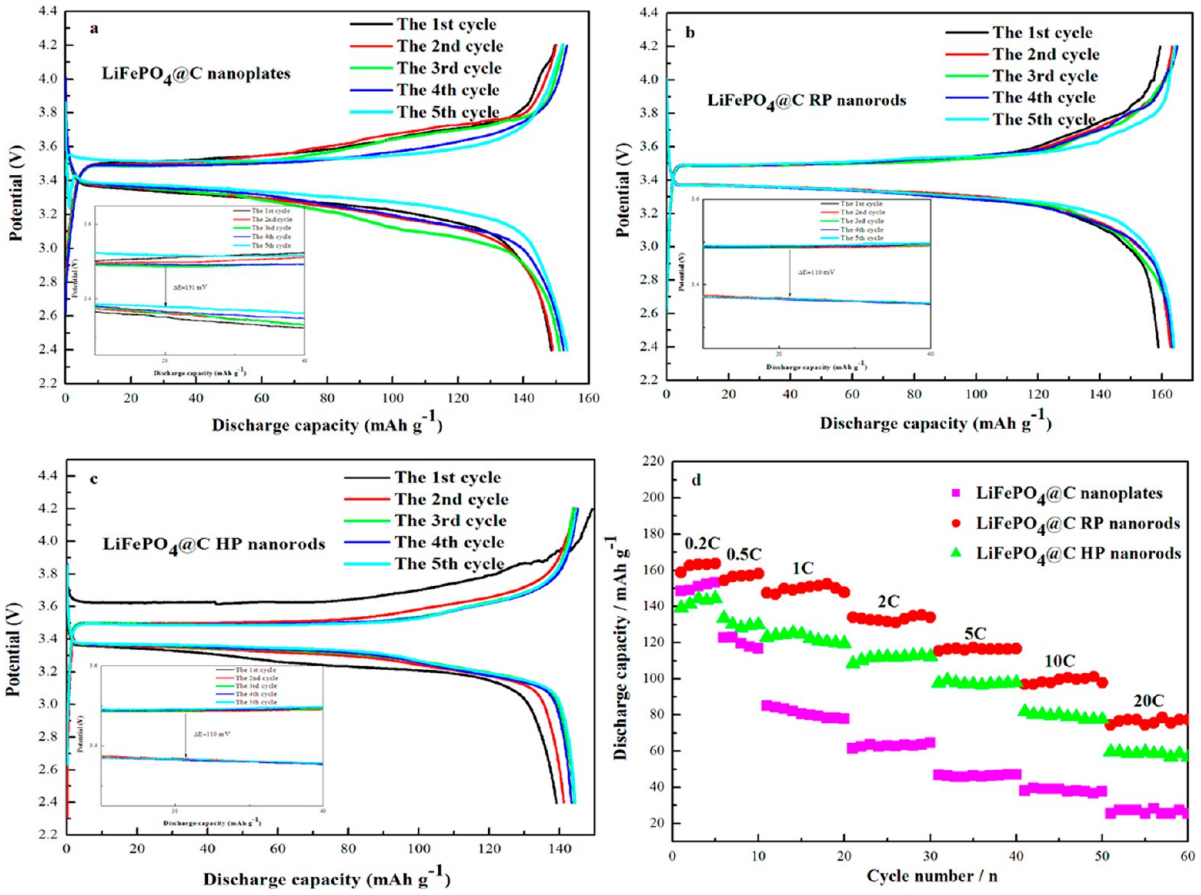

Figure 6. Electrochemical performances of $LiFePO_4$@C nanoplates, rectangular prism-like nanorods (RP nanorods) and hexagonal prism-like nanorods (HP nanorods).

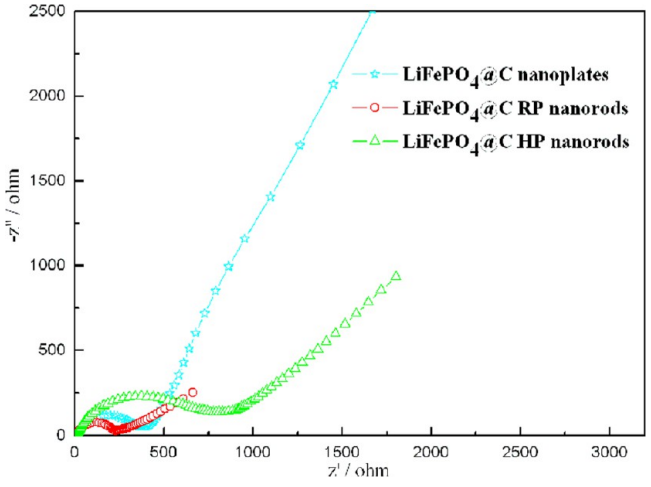

Figure 7. EIS measurements of $LiFePO_4$@C nanoplates, rectangular prism-like nanorods and hexagonal prism-like nanorods.

(glycerol-to-water ratio of 8:1), the morphology of the materials turns into nanoplates with an average length of 120 nm and width of 90 nm. Only a few nanorods are left, as shown in Figure 8c,d. With further increasing the ratio of glycerol to water to 1:1, the morphology of the materials is entirely transformed into nanorods with a mean diameter of 100 nm and length of 500 nm. A slight few of the nanorods are with wedge angles at both ends (Fig 8e,f). The HRTEM (high-resolution transmission electron microscopy) image (inset image in Figure 8f) suggests that each nanorod is a $LiFePO_4$ single crystal with a short *b*-axis and an elongation along the [001] direction. However, when the ratio is increased to 1:3, most of the materials exist as nanorods with wedge angles at both ends, but the diameter of the nanorods is slightly increased (Figure 8g,h). As the ratio increases to 0:2, the nanorods obviously grow wider, and almost all the nanorods show the wedge angles at both ends as shown in Figure 8i,j. The HRTEM in Figure 8j indicates that the plane of the wedge angles is (201) facet and the nano-hexahedral rods of the olivine $LiFePO_4$ grow preferentially along the *c*-direction. On the basis of the above observations, it can be concluded that water plays an important role in the morphology transformation of the olivine $LiFePO_4$ from nanplates to nanorods.

Figure 9 shows the XRD patterns of these samples prepared in solvents with different compositions. It is very clear that all the peaks of the $LiFePO_4$ samples obtained in different solvents can be well indexed to an orthorhombic olivine-type phase $LiFePO_4$ (JCPDS card No. 83-2092), indicating that the solvent composition has no effect on phase purity. In addition, the diffraction intensities of all the prepared $LiFePO_4$ samples gradually become stronger with the increase of the water content. This conforms that the introduction of water into the solvent system significantly benefits the crystallinity of the $LiFePO_4$.

On the basis of the above experimental results, a geometry transformation mechanism of $LiFePO_4$ particles is proposed and schematically illustrated in Figure 10. For a crystal in its thermodynamic equilibrium shape, the relative area of each

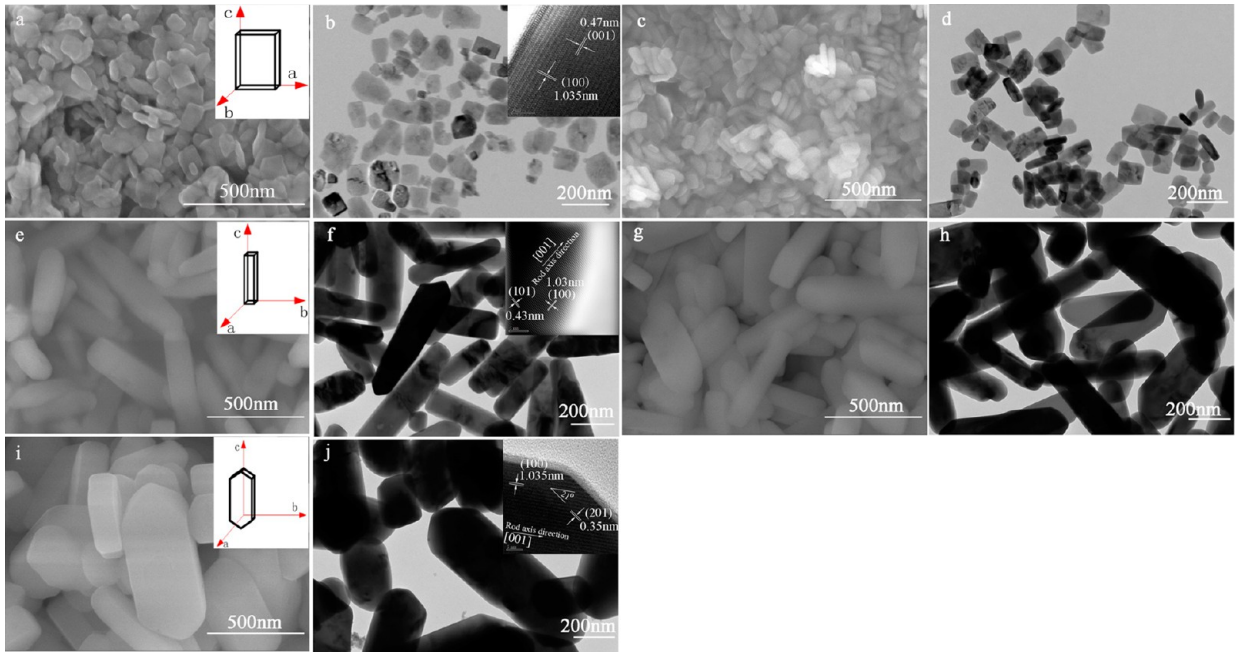

Figure 8. SEM and TEM images of these samples prepared in different solvent compositions with various volume ratios of glycerol to water of 2:0 (a, b), 8:1 (c, d), 1:1 (e, f), 1:3 (g, h), and 0:2 (i, j). The inset images in b, f, and j are the corresponding HRTEM images.

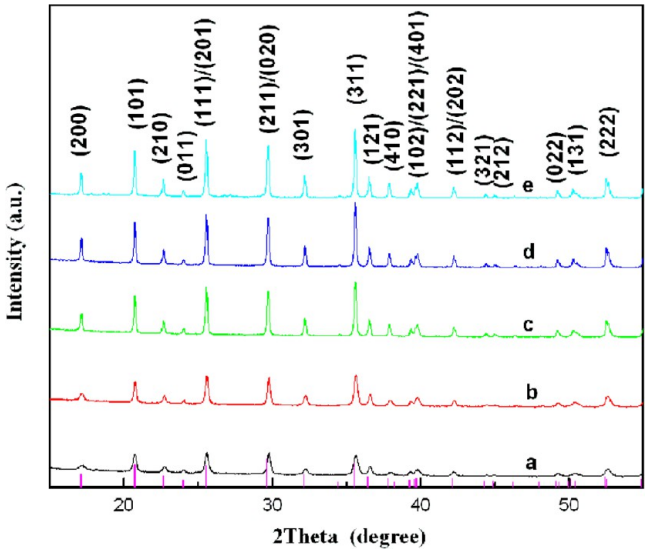

Figure 9. XRD patterns of these samples prepared in different solvent compositions with various volume ratios of glycerol to water of 2:0 (a), 8:1 (b), 1:1 (c), 1:3 (d), and 0:2 (e).

facet depends on its surface energy. When the solvent is glycerol, which is organic with three hydroxyls in each molecule, the glycerol solvent can easily adsorb on the formed $LiFePO_4$ nanocrystallites by hydrogen bonds between the hydroxyls and the oxygen atoms in each crystal facet. The adsorption of glycerol inhibits the growth of the $LiFePO_4$ crystals. Here, the surface energies of the $LiFePO_4$ in low index directions and the number of oxygen atoms in each crystal facet obtained according to Ceder's report are shown in Table 1.[49] It can be seen apparently from Table 1 that the (010) facet of the olivine $LiFePO_4$ has a relatively low surface energy and mostly oxygen atoms. On the basis of the above analysis, we propose that the glycerol solvent can be easily adsorbed on the (010) plane by hydrogen bonds between hydroxyls and oxygen atoms. Therefore, $LiFePO_4$ nanoplates with larger (010) facets are obtained by the glycerol solvent. Previous literature reported that polyhydroxy alcohol was a favorable solvent for the nanoparticles to grow into nanoplates.[50,51] However, when an appropriate amount of water is introduced into the solvent system, the selective adsorption of one hydroxyl of water is more flexible than that in three hydroxyls of glycerol. Therefore, the (010) and (100) surfaces of $LiFePO_4$ are easily adsorbed by water molecular with hydrogen bonds. Thus, the presence of water in the solvent leads to the growth of the $LiFePO_4$ nanorods with a short *b*-axis and the elongation along the [001] direction. Several groups have reported the synthesis of $LiFePO_4$ nanoparticles with anisotropic morphologies (for example, thin hexagonal platelets,[52] rectangular prisms,[53] diamond-like[54] and rods[50,55]) by hydrothermal method. Most of these nanoparticles elongate along the *c*-axis, suggesting the favorable growth in the [010] direction under normal hydrothermal reactions.[56] According to semiempirical calculations of surface energies, the stable growth morphology under mild hydrothermal conditions is close to hexagonal prism terminated by (010), (100) and (101) plane.[57] Ceder et al.[49] have calculated the thermodynamic equilibrium shape of the $LiFePO_4$ crystal based on a Wulff construction. The two low energy surfaces (010) and (201) dominate in the Wulff shape and make up almost 85% of the surface area. Both of the above calculations theoretically predict the thermodynamic stable morphologies of $LiFePO_4$ and indicate that the surface energies of the (010) and (100) faces are less than that of the (001) face. Hence, when the reaction solvent is pure water, the water molecular is favorably adsorbed in the (100), (010) and (201) planes of $LiFePO_4$ by hydrogen bonds because of more oxygen atoms on these faces. The Adsorption slows down the crystal growth along the three directions. However, the speed of the crystal growth along [001] direction is fast because of the high surface energy. Consequently, crystals that are similar to the thermodynamic equilibrium shape of the $LiFePO_4$ crystal with

dx.doi.org/10.1021/am501373h | ACS Appl. Mater. Interfaces 2014, 6, 9236−9244

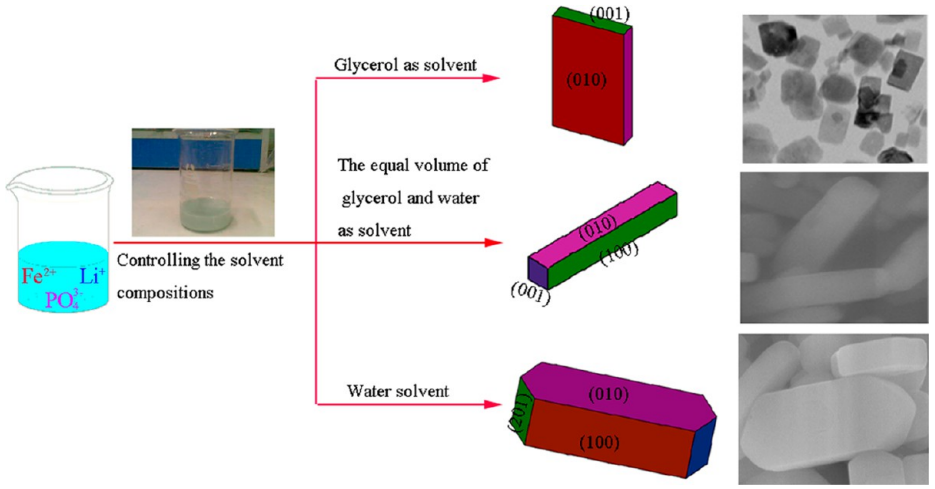

Figure 10. Schematic illustration showing the effects of the solvent compositions on the morphological transformations of $LiFePO_4$ nanoparticles during the solvothermal reaction.

Table 1. Surface Energies of $LiFePO_4$ in Low Index Direction and the Number of Oxygen Atoms in Each Crystal Facet

Miller index of $LiFePO_4$	(100)	(010)	(001)	(101)	(201)
surface energies of $LiFePO_4$ ($J\ m^{-2}$)	0.66	0.64	0.97	0.62	0.52
number of oxygen atoms	4	4	1	3	2

large (010) and (201) planes are formed with a morphology of hexagonal prism nanorod with a short *b*-axis and a long *c*-axis.

4. CONCLUSIONS

Olivine lithium iron phosphate ($LiFePO_4$) nanoplates with a larger (010) facet and rectangular prism and hexagonal prism nanorods with short *b*-axis and elongated *c*-axis are successfully synthesized via a solvothermal strategy in a glycerol and water solvent system. The morphology of the materials is closely dependent on the solvent composition. By monitoring the morphologies of $LiFePO_4$ nanoparticles prepared in solvents with different compositions, it is found that the presence of water in the solvent plays an important role in the transformation of the morphology from nanoplate to nanorod. Eventually, it changes to a thermodynamic equilibrium shape, which is similar to that of the theoretical prediction. The $LiFePO_4$@C rectangular prism nanorods exhibit very high capability and excellent rate performance. This desirable electrochemical performance is ascribed to their moderate size and shorter Li^+ ion diffusion length along the [010] direction.

■ ASSOCIATED CONTENT

Supporting Information

SEM images of the $LiFePO_4$ nanoplates, rectangular prism-like nanorods and hexagonal prism-like nanorods. Raman spectra of the $LiFePO_4$ nanoplates, rectangular prism-like nanorods and hexagonal prism-like nanorods before and after coating carbon. TGA curves of the $LiFePO_4$@C nanoplates, rectangular prism-like nanorods and hexagonal prism-like nanorods. This material is available free of charge via the Internet at http://pubs.acs.org.

■ AUTHOR INFORMATION

Corresponding Author

*Prof. Guangjie Shao. Tel.: 0086-335-8061569. Fax: 0086-335-8059878. E-mail: shaoguangjie@ysu.edu.cn.

Notes

The authors declare no competing financial interest.

■ ACKNOWLEDGMENTS

We are grateful for the financial support from the Natural Science Foundation of Hebei Province (B2012203069, B2012203070) and support from education department of Hebei province on natural science research key projects for institution of higher learning (ZH2011228)

■ REFERENCES

(1) Yonemura, M.; Yamada, A.; Takei, Y.; Sonoyama, N.; Kanno, R. Comparative Kinetic Study of Olivine Li_xMPO_4 (M=Fe, Mn). *J. Electrochem. Soc.* **2004**, *151*, A1352−A1356.

(2) Padhi, A. K.; Nanjundaswamy, K. S.; Goodenough, J. B. Phospho-Olivines as Positive-Electrode Materials for Rechargeable Lithium Batteries. *J. Electrochem. Soc.* **1997**, *144*, 1188−1194.

(3) Wang, G. X.; Bewlay, S.; Yao, J.; Ahn, J. H.; Dou, S. X.; Liu, H. K. Characterization of $LiM_xFe_{1-x}PO_4$ (M=Mg, Zr, Ti) Cathode Materials Prepared by the Sol-Gel Method. *Electrochem. Solid State Lett.* **2004**, *7*, A503−A506.

(4) Julien, C. M.; Zaghib, K.; Mauger, A.; Massot, M.; Ait-Salah, A.; Selmane, M.; Gendron, F. Characterization of the Carbon Coating ontoLiFePO$_4$ Particles Used in Lithium Batteries. *J. Appl. Phys.* **2006**, *100*, 063511−1−063511−7.

(5) Huang, H.; Yin, S. C.; Nazar, L. F. Approaching Theoretical Capacity of $LiFePO_4$ at Room Temperature at High Rates. *Electrochem. Solid State Lett.* **2001**, *4*, A170−A172.

(6) Sauvage, F.; Baudrin, E.; Gengembre, L.; Tarascon, J. M. Effect of Texture on the Electrochemical Properties of $LiFePO_4$ Thin Films. *Solid State Ionics* **2005**, *176*, 1869−1876.

(7) MacNeil, D. D.; Lu, Z.; Chen, Z.; Dahn, J. R. A Comparison of the Electrode/Electrolyte Reaction at Elevated Temperatures for Various Li-Ion Battery Cathodes. *J. Power Sources* **2002**, *108*, 8−14.

(8) Takahashi, M.; Tobishima, S. I.; Takei, K.; Sakurai, Y. Reaction Behavior of $LiFePO_4$ as a Cathode Material for Rechargeable Lithium Batteries. *Solid State Ionics* **2002**, *148*, 283−289.

(9) Yuan, L. X.; Wang, Z. H.; Zhang, W. X.; Hu, X. L.; Chen, J. T.; Huang, Y. H.; Goodenough, J. B. Development and Challenges of $LiFePO_4$ Cathode Material for Lithium-Ion Batteries. *Energy Environ. Sci.* **2011**, *4*, 269−284.

(10) Wang, Y. G.; He, P.; Zhou, H. S. Olivine $LiFePO_4$: Development and Future. *Energy Environ. Sci.* **2011**, *4*, 805−817.
(11) Hu, Y. S.; Guo, Y. G.; Dominko, R.; Gaberscek, M.; Jamnik, J.; Maier, J. Improved Electrode Performance of Porous $LiFePO_4$ Using RuO_2 as an Oxidic Nanoscale Interconnect. *Adv. Mater.* **2007**, *19*, 1963−1966.
(12) Kang, B.; Ceder, G. Battery Materials for Ultrafast Charging and Discharging. *Nature* **2009**, *458*, 190−193.
(13) Wu, X. L.; Jiang, L. Y.; Cao, F. F.; Guo, Y. G.; Wan, L. J. $LiFePO_4$ Nanoparticles Embedded in a Nanoporous Carbon Matrix: Superior Cathode Material for Electrochemical Energy-Storage Devices. *Adv. Mater.* **2009**, *21*, 2710−2714.
(14) Sun, C.; Rajasekhara, S.; Goodenough, J. B.; Zhou, F. Monodisperse Porous $LiFePO_4$ Microspheres for a High Power Li-Ion Battery Cathode. *J. Am. Chem. Soc.* **2011**, *133*, 2132−2135.
(15) Wang, Y.; Hosono, E.; Wang, K.; Zhou, H. The Design of a $LiFePO_4$/Carbon Nanocomposite With a Core−Shell Structure and Its Synthesis by an In Situ Polymerization Restriction Method. *Angew. Chem., Int. Ed.* **2008**, *47*, 7461−7465.
(16) Oh, S. W.; Myung, S. T.; Oh, S. M.; Oh, K. H.; Amine, K.; Scrosati, B.; Sun, Y. K. Double Carbon Coating of $LiFePO_4$ as High Rate Electrode for Rechargeable Lithium Batteries. *Adv. Mater.* **2010**, *22*, 4842−4845.
(17) Wang, G.; Liu, H.; Liu, J.; Qiao, S.; Lu, G. M.; Munroe, P.; Ahn, H. Mesoporous $LiFePO_4$/C Nanocomposite Cathode Materials for High Power Lithium Ion Batteries with Superior Performance. *Adv. Mater.* **2010**, *22*, 4944−4948.
(18) Liu, H.; Cao, Q.; Fu, L. J.; Li, C.; Wu, Y. P.; Wu, H. Q. Doping Effects of Zinc on $LiFePO_4$ Cathode Material for Lithium Ion Batteries. *Electrochem. Commun.* **2006**, *8*, 1553−1557.
(19) Bilecka, I.; Hintennach, A.; Rossell, M. D.; Xie, D.; Novak, P.; Niederberger, M. Microwave-Assisted Solution Synthesis of Doped $LiFePO_4$ with High Specific Charge and Outstanding Cycling Performance. *J. Mater. Chem.* **2011**, *21*, 5881−5890.
(20) Cheng, F.; Wang, S.; Lu, A. H.; Li, W. C. Immobilization of Nanosized $LiFePO_4$ Spheres by 3D Coralloid Carbon Structure with Large Pore Volume and Thin Walls for High Power Lithium-Ion Batteries. *J. Power Sources* **2013**, *229*, 249−257.
(21) Jiang, Y.; Liao, S.; Liu, Z.; Xiao, G.; Liu, Q.; Song, H. High Performance $LiFePO_4$ Microsphere Composed of Nanofibers with an Alcohol-Thermal Approach. *J. Mater. Chem. A* **2013**, *1*, 4546−4551.
(22) Lee, M. H.; Kim, T. H.; Kim, Y. S.; Song, H. K. Precipitation Revisited: Shape Control of $LiFePO_4$ Nanoparticles by Combinatorial Precipitation. *J. Phys. Chem. C* **2011**, *115*, 12255−12259.
(23) Wang, L.; He, X.; Sun, W.; Wang, J.; Li, Y.; Fan, S. Crystal Orientation Tuning of $LiFePO_4$ Nanoplates for High Rate Lithium Battery Cathode Materials. *Nano Lett.* **2012**, *12*, 5632−5636.
(24) Su, J.; Wu, X. L.; Yang, C. P.; Lee, J. S.; Kim, J.; Guo, Y. G. Self-Assembled $LiFePO_4$/C Nano/Microspheres by Using Phytic Acid as Phosphorus Source. *J. Phys. Chem. C* **2012**, *116*, 5019−5024.
(25) Zhang, C.; He, X.; Kong, Q.; Li, H.; Hu, H.; Wang, H.; Gu, L.; Wang, L.; Cui, G.; Chen, L. A Novel Assembly of $LiFePO_4$ Microspheres from Nanoplates. *CrystEngComm* **2012**, *14*, 4344−4349.
(26) Qin, X.; Wang, J.; Xie, J.; Li, F.; Wen, L.; Wang, X. Hydrothermally Synthesized $LiFePO_4$ Crystals with Enhanced Electrochemical Properties: Simultaneous Suppression of Crystal Growth along [010] and Antisite Defect Formation. *Phys. Chem. Chem. Phys.* **2012**, *14*, 2669−2677.
(27) Yang, S.; Zhou, X.; Zhang, J.; Liu, Z. Morphology-Controlled Solvothermal Synthesis of $LiFePO_4$ as a Cathode Material for Lithium-Ion Batteries. *J. Mater. Chem.* **2010**, *20*, 8086−8091.
(28) Li, J.; Qu, Q.; Zhang, L.; Zhang, L.; Zheng, H. A Monodispersed Nano-Hexahedral $LiFePO_4$ with Improved Power Capability by Carbon-Coatings. *J. Alloy. Compd.* **2013**, *579*, 377−383.
(29) Liang, Y. P.; Li, C. C.; Chen, W. J.; Lee, J. T. Hydrothermal Synthesis of Lithium Iron Phosphate using Pyrrole as an Efficient Reducing Agent. *Electrochim. Acta* **2013**, *87*, 763−769.
(30) Chen, Q.; Qiao, X.; Peng, C.; Zhang, T.; Wang, Y.; Wang, X. Electrochemical Performance of Electrospun $LiFePO_4$/C Submicro-fibers Composite Cathode Material for Lithium Ion Batteries. *Electrochim. Acta* **2012**, *78*, 40−48.
(31) Cho, M. Y.; Kim, K. B.; Lee, J. W.; Kim, H.; Kim, H.; Kang, K.; Roh, K. C. Defect-Free Solvothermally Assisted Synthesis of Microspherical Mesoporous $LiFePO_4$/C. *RSC Adv.* **2013**, *3*, 3421−3427.
(32) Gu, Y.; Liu, W.; Wang, L.; Li, G.; Yang, Y. Synthesis of 3D-Hiearchical $LiMPO_4$ (M = Fe, Mn) Microstructures as Cathode Materials for Lithium-Ion Batteries. *CrystEngComm* **2013**, *15*, 4865−4870.
(33) Zhou, N.; Uckaker, E.; Wang, H. Y.; Zhang, M.; Liu, S. Q.; Liu, Y. N.; Wu, X.; Cao, G.; Li, H. Additive-Free Solvothermal Synthesis of Hierarchical Flower-Like $LiFePO_4$/C Mesocrystal and Its Electrochemical Performance. *RSC Adv.* **2013**, *3*, 19366−19374.
(34) Wang, Q.; Deng, S. X.; Wang, H.; Xie, M.; Liu, J. B.; Yan, H. Hydrothermal Synthesis of Hierarchical $LiFePO_4$ Microspheres for Lithium Ion Battery. *J. Alloy. Compd.* **2013**, *553*, 69−74.
(35) Zhou, N.; Wang, H. Y.; Uchaker, E.; Zhang, M.; Liu, S. Q.; Liu, Y. N.; Cao, G. Additive-Free Solvothermal Synthesis and Li-Ion Intercalation Properties of Dumbbell-Shaped $LiFePO_4$/C Mesocrystals. *J. Power Sources* **2013**, *239*, 103−110.
(36) Xiao, P.; Lai, M. O.; Lu, L. Hollow Microspherical $LiFePO_4$/C Synthesized from a Novel Multidentate Phosphonate Complexing Agent. *RSC Adv.* **2013**, *3*, 5127−5130.
(37) Lee, M. H.; Kim, J. Y.; Song, H. K. A Hollow Sphere Secondary Structure of $LiFePO_4$ Nanoparticles. *Chem. Commun.* **2010**, *46*, 6795−6797.
(38) Deng, H.; Jin, S.; Zhan, L.; Qiao, W.; Ling, L. Nest-Like $LiFePO_4$/C Architectures for High Performance Lithium Ion Batteries. *Electrochim. Acta* **2012**, *78*, 633−637.
(39) Deng, H.; Jin, S.; Zhan, L.; Wang, Y.; Qiao, W.; Ling, L. Synthesis of Cage-Like $LiFePO_4$/C Microspheres for High Performance Lithium Ion Batteries. *J. Power Sources* **2012**, *220*, 342−347.
(40) Islam, M. S.; Driscoll, D. J.; Fisher, C. A. J.; Slater, P. R. Atomic-Scale Investigation of Defects, Dopants, and Lithium Transport in the $LiFePO_4$ Olivine-Type Battery Material. *Chem. Mater.* **2005**, *20*, 5085−5092.
(41) Morgan, D.; Van der Ven, A.; Ceder, G. Li Conductivity in Li_xMPO_4 (M=Mn, Fe, Co, Ni) Olivine Materials. *Electrochem. Solid-State Lett.* **2004**, *7*, A30−A32.
(42) Nishimura, S.; Kobayashi, G.; Ohoyama, K.; Kanno, R.; Yashima, M.; Yamada, A. Experimental Visualization of Lithium Diffusion in Li_xFePO_4. *Nat. Mater.* **2008**, *9*, 707−711.
(43) Xu, G.; Li, F.; Tao, Z.; Wei, X.; Liu, Y.; Li, X.; Ren, Z.; Shen, G.; Han, G. Monodispersed $LiFePO_4$@C Core−Shell Nanostructures for a High Power Li-Ion Battery Cathode. *J. Power Sources* **2014**, *246*, 696−702.
(44) Jiang, J.; Feng, Y.; Mahmood, N.; Liu, F.; Hou, Y. SnS_2/Graphene Composites: Excellent Anode Materials for Lithium Ion Battery and Photolysis Catalysts. *Sci. Adv. Mater.* **2013**, *5*, 1667−1675.
(45) Rui, X.; Zhao, X.; Lu, Z.; Tan, H.; Sim, D.; Hng, H. H.; Yazami, R.; Lim, T. M.; Yan, Q. Olivine-Type Nanosheets for Lithium Ion Battery Cathodes. *ACS Nano* **2013**, *7*, 5637−5646.
(46) Malik, R.; Burch, D.; Bazant, M.; Ceder, G. Particle Size Dependence of the Ionic Diffusivity. *Nano Lett.* **2010**, *10*, 4123−4127.
(47) Liu, J.; Jiang, R.; Wang, X.; Huang, T.; Yu, A. The Defect Chemistry of $LiFePO_4$ Prepared by Hydrothermal Method at Different pH Values. *J. Power Sources* **2009**, *194*, 536−540.
(48) Molenda, J.; Ojczyk, W.; Marzec, J. Electrical Conductivity and Reaction with Lithium of $LiFe_{1-y}Mn_yPO_4$ Olivine-Type Cathode Materials. *J. Power Sources* **2007**, *174*, 689−694.
(49) Wang, L.; Zhou, F.; Meng, Y. S.; Ceder, G. First-Principles Study of Surface Properties of $LiFePO_4$: Surface Energy, Structure, Wulff Shape, and Surface Redox Potential. *Phys. Rev. B* **2007**, *76*, 165435.
(50) Saravanan, K.; Reddy, M. V.; Balaya, P.; Gong, H.; Chowdari, B. V. R.; Vittal, J. J. Storage Performance of $LiFePO_4$ Nanoplates. *J. Mater. Chem.* **2009**, *19*, 605−610.

(51) Wang, Y. L.; Jiang, X. C.; Xia, Y. N. A Solution-Phase, Precursor Route to Polycrystalline SnO_2 Nanowires That Can Be Used for Gas Sensing under Ambient Conditions. *J. Am. Chem. Soc.* **2003**, *125*, 16176−16177.
(52) Ellis, B.; Kan, W. H.; Makahnouk, W. R. M.; Nazar, L. F. Synthesis of Nanocrystals and Morphology Control of Hydrothermally Prepared $LiFePO_4$. *J. Mater. Chem.* **2007**, *17*, 3248−3254.
(53) Recham, N.; Dupont, L.; Courty, M.; Djellab, K.; Larcher, D.; Armand, M.; Tarascon, J. M. Ionothermal Synthesis of Tailor-Made $LiFePO_4$ Powders for Li-Ion Battery Applications. *Chem. Mater.* **2009**, *21*, 1096−1107.
(54) Dokko, K.; Koizumi, S.; Nakano, H.; Kanamura, K. Particle Morphology, Crystal Orientation, and Electrochemical Reactivity of $LiFePO_4$ Synthesized by the Hydrothermal Method at 443 K. *J. Mater. Chem.* **2007**, *17*, 4803−4810.
(55) Murugan, A. V.; Muraliganth, T.; Manthiram, A. Comparison of Microwave Assisted Solvothermal and Hydrothermal Syntheses of $LiFePO_4$/C Nanocomposite Cathodes for Lithium Ion Batteries. *J. Phys. Chem. C* **2008**, *112*, 14665−14671.
(56) Uchiyama, H.; Imai, H. Preparation of $LiFePO_4$ Mesocrystals Consisting of Nanorods through Organic-Mediated Parallel Growth from a Precursor Phase. *Cryst. Growth Des.* **2010**, *10*, 1777−1781.
(57) Fisher, C. A.; Islam, M. S. Surface Structures and Crystal Morphologies of $LiFePO_4$: Relevance to Electrochemical Behaviour. *J. Mater. Chem.* **2008**, *18*, 1209−1215.